Using the Alkynyl-Substituted Rhenium(I) Complex (4,4′-Bisphenyl-Ethynyl-2,2′-Bipyridyl)Re(CO)₃Cl as Catalyst for CO₂ Reduction—Synthesis, Characterization, and Application

Engelbert Portenkirchner · Stefanie Schlager · Dogukan Apaydin · Kerstin Oppelt ·
Markus Himmelsbach · Daniel A. M. Egbe · Helmut Neugebauer · Günther Knör ·
Tsukasa Yoshida · Niyazi Serdar Sariciftci

Abstract The synthesis, structure, photophysics, and spectroscopic characterization of an organometallic rhenium multichromophore compound carrying a central 2,2′-bipyridyl acceptor moiety with additional phenylethynyl substituents conjugated at the 4,4′-positions of the acceptor ligands and its effect on the electron density of the central rhenium atom as metal center for CO_2 reduction is reported. The results were compared to *fac*-(2,2′-bipyridyl)Re(CO)₃Cl and *fac*-(5,5′-bisphenylethynyl-2,2′-bipyridyl)Re(CO)₃Cl. Cyclovoltammetric studies and rotating disk electrochemistry were performed for electrochemical characterization. Ultraviolet and visible (UV-vis) absorption, Fourier transform infrared (FTIR), and luminescence measurements were carried out for a spectroscopic characterization and compared to theoretical calculations at the density functional theory (DFT) level. In addition, the rhenium complex *fac*-(4,4′-bisphenyl-ethynyl-2,2′-bipyridyl)-Re(CO)₃Cl was used as a novel catalyst for the electrochemical reduction of CO_2 in homogeneous solution. Results showed an 11-fold increase in the current density under CO_2 saturation and a catalytic second-order rate constant for CO formation of about 560 M^{-1} s^{-1} on a Pt working electrode. For further characterization of the CO_2 reduction capabilities, bulk controlled potential electrolysis experiments were performed using a CO_2-saturated acetonitrile electrolyte solution. The headspace product gas analysis yields CO as main reduction product with faradaic efficiencies of about 12 % over 5-h electrolysis time.

E. Portenkirchner (✉) · S. Schlager · D. Apaydin · D. A. M. Egbe ·
H. Neugebauer · N. S. Sariciftci
Linz Institute for Organic Solar Cells (LIOS), Physical Chemistry,
Johannes Kepler University Linz, Altenbergerstr 69, 4040 Linz,
Austria
e-mail: Engelbert.Portenkirchner@jku.at

E. Portenkirchner
e-mail: Engelbert.Portenkirchner@uibk.ac.at

K. Oppelt · G. Knör
Institute of Inorganic Chemistry, Center for Nanobionics and
Photochemical Sciences (CNPS), Johannes Kepler University Linz,
Altenbergerstr 69, 4040 Linz, Austria

M. Himmelsbach
Institute of Analytical Chemistry, Johannes Kepler University Linz,
Altenbergerstr 69, 4040 Linz, Austria

T. Yoshida
Research Center for Organic Electronics (ROEL), Yamagata
University, Yonezawa 992-8510, Japan

Introduction

The dependence of human energy supply on limited fossil fuel resources alongside the increasing emission of carbon dioxide, which is considered a main greenhouse gas, has raised significant scientific interest in the capture and utilization of carbon dioxide [1–3]. The reduction of atmospheric carbon dioxide to synthetic carbon neutral fuels with renewable energy sources is an especially promising approach to overcome these problems [4–6].

Organometallic rhenium(I) bipyridine (bpy) complexes have received substantial interest in the research field of

homogeneous electro- and photocatalysts for CO_2 reduction due to their high efficiency, stability, and product selectivity. Studies show that these catalysts yield CO as the main reduction product with almost no hydrogen and formic acid formed as side products [7–10]. It has been shown that the metal-centered and the metal-to-ligand charge-transfer (MLCT) electronic states can be altered by ligand modification [11, 12]. Recently, our group reported the synthesis, structure, photophysics, spectroscopic characterization, and catalytic activity of the modified rhenium complex (5,5′-bisphenylethynyl-2,2′-bipyridyl)Re(CO)$_3$Cl, carrying additional phenylethynyl substituents at the acceptor ligand on the 5,5′-position compared to the well-studied (2,2′-bipyridyl)-Re(CO)$_3$Cl [11, 13]. This new compound has an extended conjugated π-electron system that shifts the optical absorption of the intraligand bands into the visible spectral range which is considered an important benefit for potential photocatalytic applications.

In the present study, the results obtained for compound (1) are compared to our previous findings for (2) and (3), depicted in Scheme 1, showing the effect of additional phenylethynyl substituents at the acceptor ligand 4,4′-position. It is expected that this substitution in *para*-position to the metal binding site in addition to the situation in (2) also leads to a more pronounced delocalization of π-electron density involving the central rhenium atom and hence influences the catalyst activity towards electro- and photocatalytic CO_2 reduction. Ultraviolet and visible (UV-vis) absorption, Fourier transform infrared (FTIR), and photoluminescence (PL) measurements were carried out for a spectroscopic characterization and compared to theoretical ab initio calculations at the density
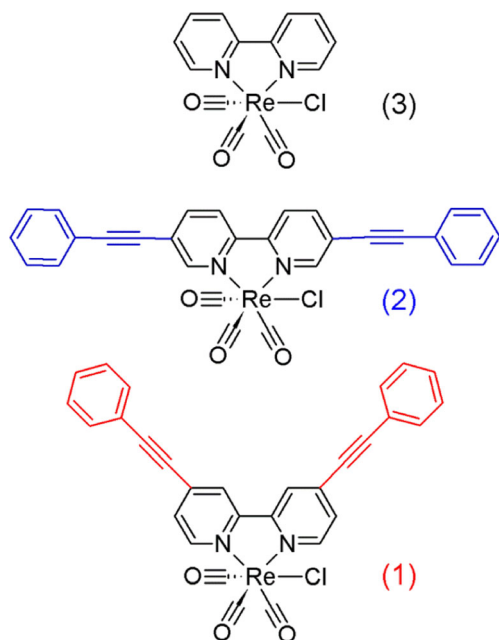
Scheme 1 Chemical structures of (4,4′-bisphenylethynyl-2,2′-bipyridyl)Re(CO)$_3$Cl (1), (5,5′-bisphenylethynyl-2,2′-bipyridyl)-Re(CO)$_3$Cl (2), and (2,2′-bipyridyl)Re(CO)$_3$Cl (3)

functional theory (DFT) level. Detailed electrochemical characterization of the novel compound in organic solvents under inert N_2 atmosphere was carried out, and rotating disk experiments (RDEs) were performed. Additionally, the rhenium complex (1) was used as a novel catalyst for the electrochemical reduction of CO_2 in homogeneous solution. For CO_2 reduction analysis, bulk controlled potential electrolysis experiments were performed using a CO_2-saturated acetonitrile solution.

Synthesis

2,2′-Bipyridine-*N*,*N*′-Dioxide (5)

Initially, 40 g of 2,2′-bipyridine (4) were dissolved in 220 mL glacial acetic acid and 140 mL hydrogen peroxide and heated under stirring for 2 h at 80 °C (Scheme 2). Additional 140 mL H_2O_2 was added dropwise, and the temperature was raised to 90 °C. The mixture was stirred for 18 h at 90 °C. After cooling to room temperature, the mixture was poured into 2.4 L of acetone for precipitation. The white crystalline solid was filtered, washed with acetone, and dried under vacuum to yield 39.5 g (214.7 mmol, 81.7 %) [14].

### 4,4′-Dinitro-2,2′-Bipyridine-*N*,*N*′-Dioxide (6)

For this step, 9 g of compound (5) was dissolved in a mixture of 26 mL 95 % sulfuric acid and 4 mL fuming sulfuric acid. The solution was cooled to 0 °C under stirring. Twenty milliliters of fuming nitric acid was added carefully, and the solution was heated at 100 °C for 4 h. The solution then was cooled to 0 °C and poured onto 100 g of ice. The yellow solid was filtered, washed with water, and dried under vacuum to yield 6.1 g (22.2 mmol, 45.5 %) [15].

4,4′-Dibromo-2,2′-Bipyridine-*N*,*N*′-Dioxide (7)

For the bromination reaction, 63 mL of acetyl bromide were added to a suspension of 6 g of compound (6) and 95 mL glacial acetic acid. The mixture then was heated (90 °C) for 2 h. The resulting brownish liquid was cooled to 3 °C and mixed with 200 g of ice. Two hundred fifty milliliters of 6 N NaOH was added for neutralization (~pH 6) and subsequent precipitation. The yellow to light green solid was filtered, washed with water, and dried in vacuum to yield 5.5 g (14.9 mmol, 68.2 %) [16].

4,4′-Dibromo-2,2′-Bipyridine (8)

A mixture of 1.5 g of compound (7), 10 mL PBr$_3$, and 200 mL acetonitrile was heated to reflux for 4 h at 80 °C. After cooling to room temperature, the suspension was poured onto ice and
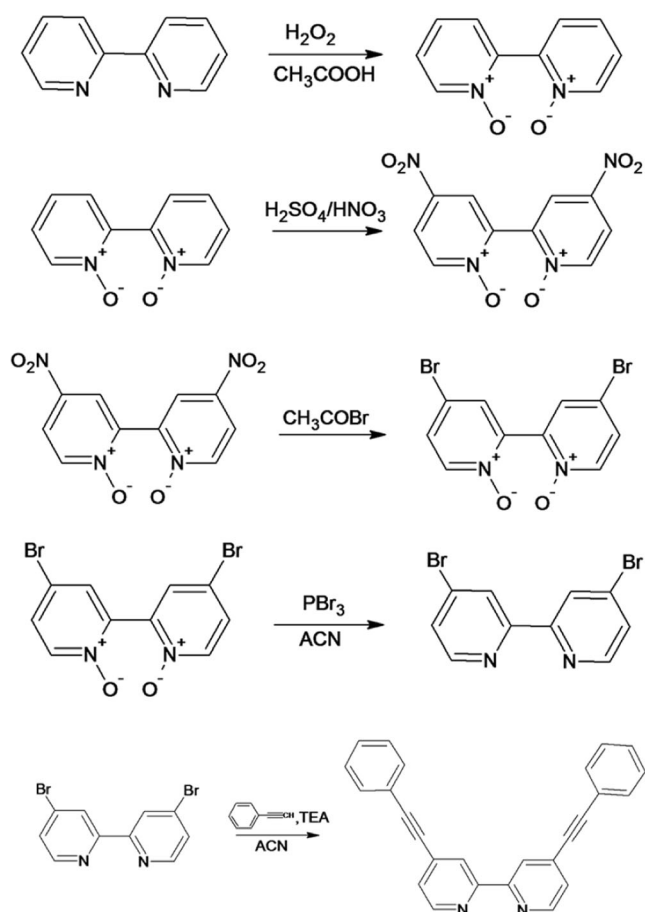
Scheme 2 Synthesis sequence from 2,2′-bipyridine (**4**) to 4,4′-bis(phenylethynylene)-2,2′-bipyridine (**9**)

the pH was adjusted to 11 with 6 N NaOH resulting in precipitation of the substance. Additionally, chloroform was added to the mixture for extraction. The solvents were removed from the organic phases to achieve a solid product. By adding 200 mL of a 1:1 mixture of ethanol and water, precipitation of the pure product was achieved. The white solid product was than filtered and dried in vacuum to yield 0.7175 g (2.1 mmol, 51.3 %) of compound (**8**) [16].

4,4′-Bis(Phenylethynylene)-2,2′-Bipyridine (**9**)

For the Sonogashira coupling reaction, compound (**8**) (0.5 g, 1.6 mmol) was added to a mixture of toluene (25 mL), phenylacetylene (1 mL), and triethylamine (1.6 mL). The mixture was degassed with nitrogen for 1 h. Subsequently, Pd(PPh$_3$)$_4$ (22 mg) and CuI (11.3 mg) were added, and the mixture was degassed for additional 10 min, then heated under reflux for 3 h. The mixture was cooled over night to room temperature and filtered to remove the inorganic salts. The filtrate was treated under vacuum to remove the solvents, and the resulting residue was purified using column chromatography on silica with a mixture of cyclohexane and tetrahydrofuran (THF) (3:1 in volume). The obtained crude product was

washed with cooled methanol and dried in vacuum to yield 0.2 g (0.54 mmol 36.4 %) of compound (**9**).

Complexation with Re

Toluene (50 mL) was heated to reflux in nitrogen atmosphere. Compound (**9**) (150 mg, 0.4 mmol) and 0.1528 g of ReCO$_5$Cl (152.8 mg, 0.5 mmol) were added slowly. After 2.5 h, the mixture was cooled. The precipitated solid was filtered and dried in vacuum to yield 0.27 g (0.41 mmol, 98.4 %) of compound (**1**).

Results and Discussion

UV-vis Absorption Spectroscopy and PL Measurements

The complex *fac*-(2,2′-bipyridyl)Re(CO)$_3$Cl (**3**) is known to be an efficient photocatalyst for the reduction of CO$_2$ producing mainly CO with the aid of a sacrificial electron donor such as triethanolamine (TEOA) [17, 18]. Suitable modifications of the ligand sphere in derivatives of (**3**) led to the development of improved systems with quantum yields (Φ_{CO}) up to 0.59, making this type of materials the most efficient CO$_2$ reduction photocatalysts known by now [7, 12]. Additionally, variations of the substitution pattern of the bipyridyl ligand should have a strong influence on the relative ordering of the lowest-lying excited states in such rhenium carbonyl complexes [19]. In our case, this is clearly reflected in the electronic spectra of the corresponding compounds. Figure 1 shows a comparison of the UV-visible absorption spectra of a dilute solution of the three different rhenium carbonyl complexes (**1**), (**2**), and (**3**) in acetonitrile. The complexes presented are (**3**) (black line), (**1**) (red line), and (**2**) (blue line), respectively.

The absorption spectra of the rhenium bipyridyl complexes exhibit strong intraligand $^1\pi\pi^*$ transitions of the diimine ligands in the higher energetic UV region. Also, these complexes usually display less intense metal-to-ligand charge transfer (MLCT) signatures at lower energies [11, 20, 21]. In acetonitrile, compound (**1**) (red line) is characterized by a broad absorption maximum at around 400 nm, red-shifted compared to (**3**) (black line) with a maximum at about 365 nm. In contrast, the spectrum of compound (**2**) (blue line) is dominated by an intraligand band at about 375 nm. Additional weaker UV bands of intraligand transition origin are occurring between 280 and 320 nm. It should be noted that the absorption features of the tricarbonylchlororhenium(I) polypyridyl complexes of the (LL)Re(CO)$_3$Cl-type are known to be sensitive to the nature of the solvent. It was found that the visible spectra of all rhenium complexes undergo a bathochromic shift with decreasing solvent polarity; therefore, slightly different values for the absorption maxima of (**2**) and
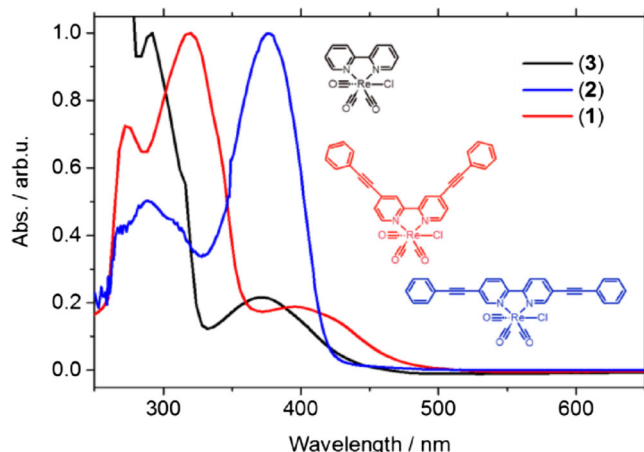
Fig. 1 Comparison of normalized UV-visible absorption spectra of three different rhenium carbonyl complexes in acetonitrile solution. The complexes are (**1**) (*red line*), (**2**) (*blue line*), and (**3**) (*black line*)

(**3**) have been reported when different solvents were used [10, 11, 20]. A normalized absorption spectra of compound (**1**) in dimethylformamide (DMF) solution can be found in the supplementary information Fig. S4.

Figure 2 shows the excitation (red solid line, λ_{PL} at 680 nm) and emission (black dashed line, λ_{exc} at 450 nm) spectrum of a dilute solution of compound (**1**) in DMF (30 μg/mL). The broad emission of the ^{3}MLCT to the ground state of the compound is covering a typical wide spectral region including orange and red light exhibiting a maximum at around 700 nm. For the excitation spectrum, the emission of the homogeneous solution was measured at λ_{PL} of 680 nm and the excitation wavelength was scanned from 350 to 650 nm.

The luminescence signal was corrected according to the amount of emitted photons by the excitation light source using an internal calibrated Si photodiode (black dashed line). Although the data were recorded in different solvents, a satisfactory agreement between the excitation spectrum of
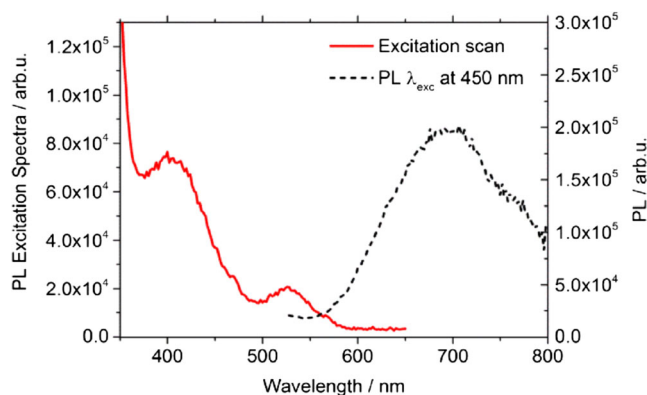
compound (**1**) in Fig. 2 and the absorption spectrum in Fig. 1 is found.

IR Spectra

The infrared (IR) spectrum of complexes of the (LL)Re(CO)$_3$Cl-type are dominated by their characteristic signals connected to the C≡O vibrations positioned at around 1900 and 2000 cm^{-1}, respectively [9, 11]. As the IR absorption bands of the C≡O vibrations are dominant in the spectra and reside in the frequency region where no other absorption bands exist, these bands are useful to probe the electronic exited states of these compounds. Additionally, these band frequencies are greatly influenced by the electron density on the central rhenium(I) atom, which is considered to be the driving force for catalytic CO$_2$ reduction [12]. In a very recent study, Kubiak and his group reported on the shift of the ν_{CO} stretching vibration upon reaction of [Re(bipy)(CO)$_3$]$^-$ and CO$_2$. Furthermore, they have been able to identify the intermediate product Re-CO$_2$H from the reaction of [Re(bipy)(CO)$_3$]$^-$ and CO$_2$ by the growth of additional ν_{OCO} stretching vibrations at 1662 and 1616 cm^{-1} with in situ stopped flow experiments [22, 23].

Since the interpretation of infrared spectra is difficult for large molecules based on measured data only, calculated infrared absorption spectra by quantum mechanical density functional theory calculations were successfully used to correlate characteristic features in the measured spectra to their molecular origin. Figure 3 shows the FTIR difference absorption spectrum of (**1**) measured in potassium bromide (KBr) (black solid line). Additionally, the corresponding calculated IR absorption spectrum (red line) is shown. The spectrum was calculated on the DFT level with the software Gaussian 09. The IR signal positioned at 2200 cm^{-1} is attributed to the C≡C vibrations of the rigid phenylethynyl substituents in their 4,4′-

Fig. 2 Excitation (*red solid line*, λ_{PL} at 680 nm) and emission (*black dashed line*, λ_{exc} at 450 nm) spectrum of compound (**1**) in DMF (30 μg/mL). The ^{3}MLCT emission spectrum is indicated by a maximum at around 700 nm
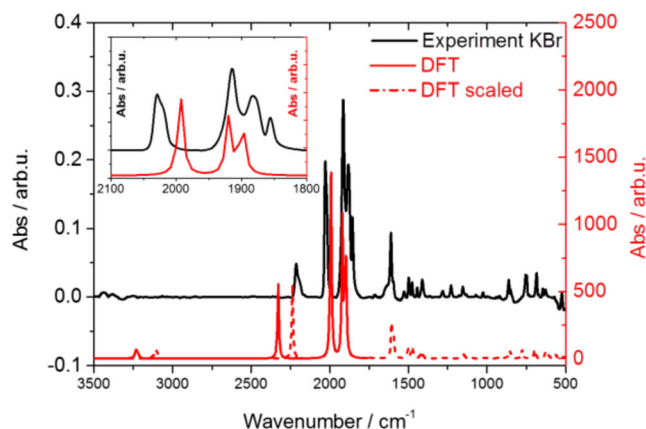

Fig. 3 FTIR difference absorption spectra of (**1**) in KBr (*black solid line*) and corresponding calculated IR absorption spectra by DFT (*red solid line*) and scaled by a constant factor of 0.9614 (*red dashed line*). The inset shows an expanded form of the main figure in the range between 2100 and 1800 cm^{-1}

position. Similar vibrations have been found in the previously reported compound (2) [24]. The signal at 1650 cm^{-1} is typical for the C=C stretching vibrations in the aromatic ligand system. The weak signals around 1500 cm^{-1} are characteristic C-H bending vibrations, and those at 880, 800, and 720 cm^{-1} are attributed to C-H rocking vibrations [25]. The inset in Fig. 3 shows an expanded form of the main figure in the range of the characteristic C≡O vibrations between 2100 and 1800 cm^{-1}.

It was found that calculated ab initio harmonic vibrational frequencies are typically larger than the fundamental vibrational frequencies observed experimentally. For the prediction of infrared spectra, it is often necessary to scale the obtained calculated data by a constant factor to achieve good matching of calculated and measured spectra. As can be seen in Fig. 3, experimentally observed data and quantum chemical predictions for the IR spectra of the compound are in good agreement. Additionally, for the prediction of the infrared spectrum shown in Fig. 3, the obtained IR data has been scaled by a constant factor of 0.9614 according to reference [26].

DFT Calculations

The charge transfer character of the absorption bands in the visible spectral region of complex (1) and related compounds is expected to dominate the excited state properties. This can be illustrated by quantum mechanical calculations, which indicate that the frontier orbital transitions are occurring mainly from the tricarbonyl rhenium(I) chloride moiety [27].

Figure 4 depicts the energy levels of the last four occupied and first four unoccupied molecular orbital (MO) of the compound (1) obtained from theoretical calculations at the DFT level. The method used for these calculations was similar to the one previously reported in reference number [11]. The calculations were carried out with the Gaussian 09 [28]. All
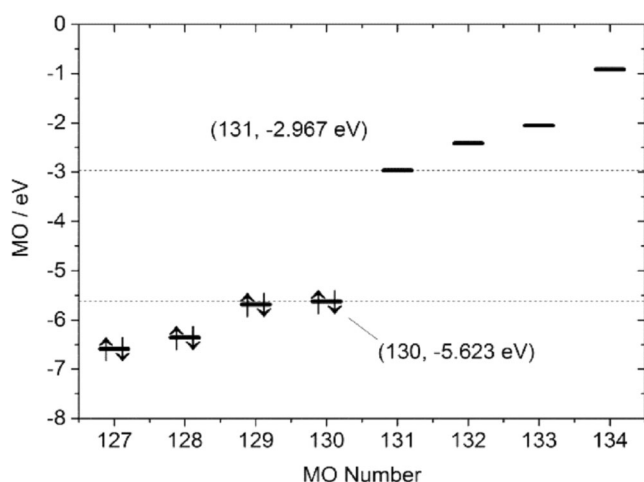

Fig. 4 Molecular orbital energy levels calculated by DFT for the frontier orbitals including HOMO-LUMO gap

quantum-chemical calculations were carried out using a density functional theory (DFT)-based method with the hybrid B3LYP functional [29, 30]. The 6-31G(d) basis set was used throughout all the calculations [31, 32], except for the complexed rhenium metal, the LanL2DZ [33] basis set was applied. The obtained geometries were verified to correspond to a real minimum by establishing an absence of imaginary IR frequencies. As can be seen in Fig. 4, quantum mechanical calculations yield the highest occupied molecular orbital (HOMO) energy level of about −5.62 eV and the lowest unoccupied molecular orbital (LUMO) energy level of about −2.97 eV for (1) resulting in a HOMO-LUMO energy difference of about 2.65 eV.

Similar calculations for the compound Re(2,2′-bpy)(CO)$_3$Cl (3) gave a larger HOMO-LUMO energy difference of 2.89 eV which is in agreement with the UV-vis absorption measurements depicted in Fig. 1.

Figure 5 shows a visual representation of molecular frontier orbitals obtained from theoretical calculations at the DFT level. The results obtained from DFT calculations are in particular interesting when compared with optical measurement, since the assignment of the lowest-lying excited states of (4,4′-bisphenylethynyl-2,2′bipyridyl)Re(CO)$_3$Cl as intraligand (IL) and metal-to-ligand charge transfer (MLCT) type is in agreement with the results obtained from the DFT calculations and with previous studies of similar compounds reported in literature [11]. As visualized in Fig. 5, the HOMO of the rhenium complex carries a significant metal d-orbital contribution from the Re(CO)$_3$Cl fragment, which determines the charge transfer character of the lowest excited states in this material. These energy states are of crucial importance for the photochemical reactivity of such systems. In a previous study, our group suggested that an inversion of this lowest-lying excited state properties of the similar compound (2) leads to a reduced photocatalytic activity towards CO$_2$ reduction compared to (3), compare reference number [13].

Electrochemical Studies

Electrochemical studies are of high importance to test and characterize a compound towards its electrocatalytic ability for CO$_2$ reduction. Especially the rate of the carbon dioxide reduction reaction is an important measure for the capability of a homogeneous catalyst if the electrochemical response is diffusion controlled. A comparison between various homogenous catalysts is generally given by the rate constant k. To define k of a diffusion controlled electrocatalytic response, rotating disk experiments are applied to first determine the diffusion coefficient D of the complex and from this calculate k [9].

Figure 6 shows the electrochemical characterization of (1) in a nitrogen-saturated electrolyte solution with a scan rate of 50 mV s^{-1}. The characteristic peaks upon reduction are

HOMO   LUMO
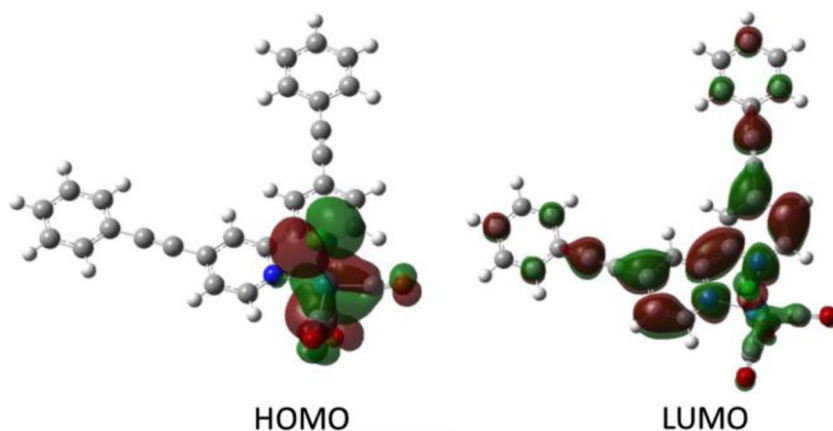
indicated with the numbers 1–6 in Fig. 6. The measurements were done in dimethylformamide (DMF) with 0.1 M TPABF$_4$ as supporting electrolyte and a glassy carbon working electrode. The catalyst concentration was 0.5 mM. For the reduction measurement (blue line) and oxidation measurement (red line), respectively, two independent cyclic scans were performed to avoid the influence of products formed due to the opposite respective bias scan. When the potential is scanned towards negative potentials with respect to the Ag/AgCl quasi-reference electrode, from 0 to −2 V, four independent reduction waves are observed with their maxima at about −0.9, −1.15, −1.6, and −1.9 V vs. Ag/AgCl, respectively.

The first reduction wave 1 at −0.9 V was poorly reproducible for its magnitude, probably arising from some impurities in the solvent system, and thus was not further considered for discussion. The second reduction peak 2 at
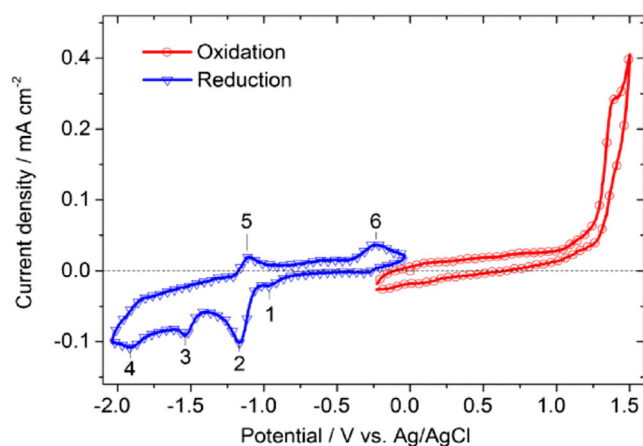

Fig. 6 Cyclic voltammograms of (**1**) in nitrogen-saturated electrolyte solution with a scan rate of 50 mV s^{-1} for reduction (*blue line*) and oxidation (*red line*), respectively. The characteristic peaks are indicated with the numbers *1–6*. Measurements are taken in dimethylformamide with 0.1 M TPABF$_4$, glassy carbon working electrode, Pt counter electrode, and a catalyst concentration of 0.5 mM

−1.15 vs. Ag/AgCl is prominent, quasi-reversible, and attributed to a ligand-based reduction similar to the behavior of the pyridine-centered first reduction of (**3**) reported by Lehn et al. in 1984 [17].

$$Re^I L(CO)_3 Cl + e^- \rightarrow \left[Re^I L^\bullet (CO)_3 Cl \right]^- \qquad (i)$$
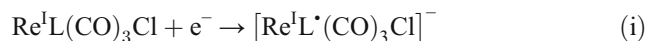
where L represents the bipyridine ligand, which is 4,4′-dibromo- 2,2′-bipyridine in the present study, while L$^\bullet$ is the anion radical of L having an extra electron in its π* orbital. Coordination of Cl$^-$ ion to the central Re ion is significantly weakened due to the presence of L$^\bullet$. Some of the reduced complexes therefore are expected to release Cl$^-$ and can undergo dimerization by forming a Re^0-Re^0 bond [34].

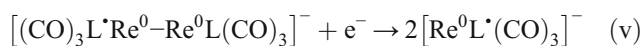$$2\left[Re^I L^\bullet (CO)_3 Cl \right]^- \rightleftharpoons (CO)_3 L Re^0 - Re^0 L(CO)_3 + 2Cl^- \quad (ii)$$

Formation of such a dimeric species could be responsible for the quasi-reversibility of reaction (i) since some amount of the reduced [Re^{I}L$^\bullet$(CO)$_3$Cl]$^-$ is used for dimerization and will not be oxidized on reversal of the potential scanning. The following reduction peak 3 at −1.6 V is clearly smaller than the second reduction peak and appears to be completely irreversible. It is attributed to a single electron reduction of the dimer species.

$$(CO)_3 L Re^0 - Re^0 L(CO)_3 + e^- \rightarrow \left[(CO)_3 L^\bullet Re^0 - Re^0 L(CO)_3 \right]^-$$
$$(iii)$$
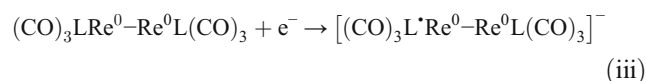
Since the number of electrons is 0.5 per Re for reaction (iii) and only a part of the reduced monomer is expected to dimerize within the timescale of the experiment, the smaller size of the cathodic peak is reasoned. The extra electron in the reduced dimer is delocalized between two ligand systems, making it fairly stable against dissociation. The fourth reduction peak at −1.9 V is broad and appears to be partially reversible. This peak should represent the second reduction of the remaining reduced monomer as well as the singly

reduced dimer, resulting both cases in formation of 5-coordinated anionic complex having L$^{\bullet}$ moiety, since they are accompanied with detachment of Cl^{-} and breaking up of the Re-Re bond, respectively.

$$\left[Re^{I}L^{\bullet}(CO)_3Cl\right]^{-} + e^{-} \rightarrow \left[Re^{0}L^{\bullet}(CO)_3\right]^{-} + Cl^{-} \qquad (iv)$$

$$\left[(CO)_3L^{\bullet}Re^{0}-Re^{0}L(CO)_3\right]^{-} + e^{-} \rightarrow 2\left[Re^{0}L^{\bullet}(CO)_3\right]^{-} \quad (v)$$

The broadness of the fourth cathodic peak can be attributed to the parallelism of reactions (iv) and (v) whose formal potentials are supposedly not far apart. It should be noted that the number of electrons per Re becomes two at the cathodic end of the potential scanning related to the abovementioned reduction sequence. This assumption approximately matches with the comparison of the peak areas, namely that of the second peak almost equals to the addition of those of the third and fourth. This is exactly supported by the quantification gained from the RDE measurements as discussed later.

The broad anodic peak 5, on reversal of the potential scanning, is attributed to the oxidation of the doubly reduced complex whose fate, however, must be highly complex since several reactions have to be considered.

$$\left[Re^{0}L^{\bullet}(CO)_3\right]^{-} + Cl^{-} \rightarrow \left[Re^{I}L^{\bullet}(CO)_3Cl\right]^{-} + e^{-} \qquad (vi)$$

$$\left[Re^{0}L^{\bullet}(CO)_3\right]^{-} + A \rightarrow \left[Re^{I}L^{\bullet}(CO)_3A\right]^{-} + e^{-} \qquad (vii)$$
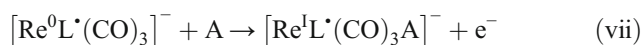
(A represents an anion other than Cl^{-})

$$\left[Re^{0}L^{\bullet}(CO)_3\right]^{-} + DMF \rightarrow Re^{I}L^{\bullet}(CO)_3(DMF) + e^{-} \qquad (8)$$

$$2\left[Re^{0}L^{\bullet}(CO)_3\right]^{-} \rightarrow \left[(CO)_3L^{\bullet}Re^{0}-Re^{0}L(CO)_3\right]^{-} + e^{-} \quad (ix)$$

The oxidation coupled to the uptake of Cl^{-} ion to regenerate the original structure of complex (vi) is highly unlikely because of the very small concentration of Cl^{-}. The oxidation to yield the half-reduced dimer (ix) is also not likely since such a chemical reaction should be kinetically slow. The absence of the anodic peak for reversal of reaction (iii) also eliminates (ix) as the main reaction pathway. Then, the reactions (vii) and (viii) are expected to represent the majority. The complexity of the reaction should be the reason for the broadness of the

anodic wave. The oxidation of the substituted species such as [Re^{I}L$^{\bullet}$(CO)$_3$A]$^{-}$ and Re^{I}L$^{\bullet}$(CO)$_3$(DMF) either coincides with that of [Re^{I}L$^{\bullet}$(CO)$_3$Cl]$^{-}$ (reversal of (i)), obscured in the cyclic voltammograms due to their broadness, or are chemically unstable to find their way to generate dimers in the course of the potential scanning.

$$2\left[Re^{I}L^{\bullet}(CO)_3A\right]^{-} \rightleftharpoons (CO)_3LRe^{0}-Re^{0}L(CO)_3 + 2A^{-} \quad (x)$$

$$2Re^{I}L^{\bullet}(CO)_3(DMF) \rightleftharpoons (CO)_3LRe^{0}-Re^{0}L(CO)_3 + 2DMF \quad (xi)$$

Finally, there is an anodic peak 6 at around −0.2 V. This should represent an oxidation of the dimer complex.

$$(CO)_3LRe^{0}-Re^{0}L(CO)_3 \rightarrow \left[(CO)_3LRe^{I}-Re^{0}L(CO)_3\right]^{+} + e^{-}$$
$$(12)$$
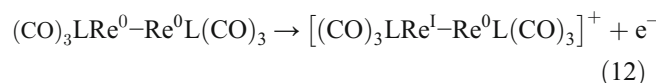
The product of this reaction may undergo further oxidation and dissociate into the monomer [34], but we did not go into further studies at this stage due to the already highly complex nature of the electrochemical reactions of this complex. It is also important to keep in mind that the ethynylene moiety of the ligand of the compound (1) of the present study may allow polymerization upon redox reactions [24] making the chemistry further complex.

When the potential is scanned to positive potentials with respect to the Ag/AgCl quasi-reference electrode (red line), (1) is irreversibly oxidized above 1.2 V vs. Ag/AgCl. Following these measurements, the electrochemical HOMO-LUMO gap of (1) is determined as 2.35 eV and hence somewhat smaller than that obtained from UV-vis absorption measurements with 2.48 eV, when 500 nm is taken as the onset for the lowest-lying absorption (Fig. 1). The differences in these values for HOMO-LUMO energies can be understood when the different methods are taken into account. In the UV-vis absorption measurement, the electron is excited within the molecule and the transition from the HOMO to the LUMO is measured. Differently, in electrochemistry, an electron is put into the system from a metal electrode to the LUMO level upon reduction and an electron is taken from the HOMO level of the molecule upon oxidation. Both techniques are used in the community for HOMO-LUMO gap determination. Additionally, quantum mechanical calculations at the DFT level yield 2.66 eV for the HOMO-LUMO gap (Fig. 4).

Figure 7 shows scan rate-dependent cyclic voltammograms of (1) in nitrogen-saturated electrolyte solution with different scan rates from 10 mV s^{-1} (brown line) to 500 mV s^{-1} (blue line), respectively. The measurements were taken under otherwise identical conditions as reported for the measurement in Fig. 6. The inset shows the linear dependence of the cathodic peak currents at −1.15, −1.6, and −1.9 V with the square root
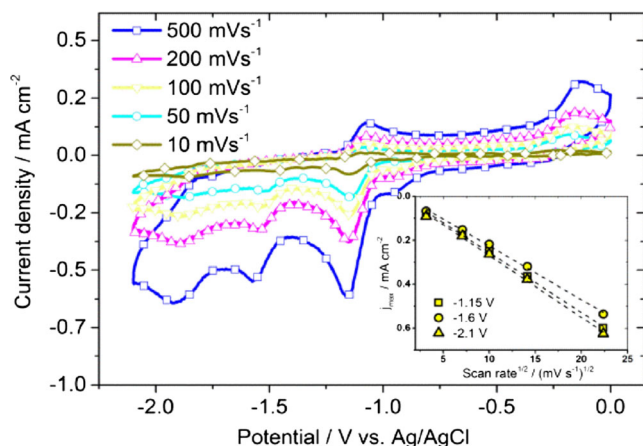
Fig. 7 Cyclic voltammograms of (**1**) in nitrogen-saturated electrolyte solution with different scan rates from 10 mV s^{-1} (*brown line*) to 500 mV s^{-1} (*blue line*), respectively. Measurements are taken in dimethylformamide with 0.1 M TPABF$_4$, glassy carbon working electrode, Pt counter electrode, and a catalyst concentration of 0.5 mM. The *inset* shows the linear dependence of the cathodic peak current at 1.15, −1.6, and −1.9 V with the square root of the scan rate from the measurements depicted in the *main figure*

of the scan rate from the measurements shown in the main figure.

This linear dependence (*R* square>0.99) of the cathodic peak currents with the square root of the scan rate indicates a diffusion-limited electrochemical reaction following the Randles-Sevcik equation [35].

$$i_{max} = (2.69 \cdot 10^5) n^{3/2} D^{1/2} \nu^{1/2} C \qquad (1)$$

where i_{max} is the maximum peak current in the unit of A cm^{-2}, n is the number of electrons, D is the diffusion coefficient, ν is the scan rate, and C is the concentration of the analyte in solution.

As mentioned in the introduction, the rate of the CO_2 reduction reaction is an important measure for the capability of a homogeneous catalyst. Comparison between various compounds is generally given by the rate constant k. To define k of a diffusion-controlled catalyst mechanism, usually rotating disk experiments are applied to determine the diffusion coefficient of the catalyst molecule [9]. From the experimental data obtained by this technique, one can apply the Levich equation to calculate the diffusion coefficient according to Eq. 2 [36, 37].

$$i_L = (0.62) nFAD^{2/3} \omega^{1/2} \nu^{-1/6} C \qquad (2)$$

where i_L is the plateau current measured from the RDE, n is the number of electrons, F is Faraday's constant, A is the electrode area, D is the diffusion coefficient, ω is the rotation rate, ν is the kinematic viscosity of the solution, and C is the

concentration of the analyte in solution. The catalytic rate constant (k) can then be extracted from Eq. 3 which holds true for a reversible electron-transfer process followed by a fast catalytic reaction [38].

$$i_C = nFA[cat]\sqrt{Dk[Q]^y} \qquad (3)$$

where i_c is the catalytic current, [*cat*] is the catalyst concentration, [*Q*] is the concentration of the substrate (in this case CO_2), y is the order of the substrate in the reaction in question, and the other parameters are the same as in Eqs. 1 and 2. Figure 8 shows the linear sweep voltammetry measured at an RDE employing glassy carbon as the electrode material. Along the I-V curves, four waves are recognized, corresponding to those seen in the cyclic voltammograms as described above. The prominent second reduction wave, corresponding to the ligand reduction according to (i) shows a quasi-plateau, while others are ill-defined. The current values measured at −1.3 V vs. Ag/AgCl for rotation rates of 200, 400, 600, 800, 1000, 1200, 1600, and 2000 rpm are taken as the limiting currents and are plotted against the square root of the rotation speed (Levich plot, shown as the inset of Fig. 3). The Levich plot demonstrates a very high linearity with a mean square error close to one ($R^2=0.9993$) and an intercept close to zero (−0.001).

Since the following two waves are not creating a plateau, probably due to slow charge transfer kinetics, steady-state current experiments at −2.1 V, corresponding to full reduction of the catalyst according to (iv), are recorded. During this measurement, the rotation rate was varied from 0 to 1400 rpm as shown in Fig. 9a. The chosen potential is addressing the fourth reduction wave (compare Fig. 6) which is
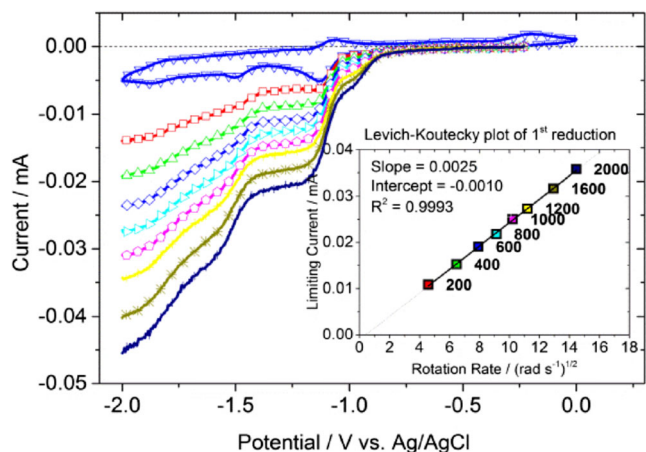

Fig. 8 Rotating disk electrode data for (**1**) with rotation rates from 200 to 2000 rpm, respectively. Measurements are taken in DMF with 0.5 mM rhenium complex, 0.1 M TPABF$_4$, a glassy carbon working electrode, platinum wire counter electrode, and Ag/AgCl reference electrode. The *inset* shows the Levich plot for the measurements depicted in the *main figure*; the color of the measurement points matches the color of the current-potential curve. Limiting current values are measured at the potential of −1.3 V vs. Ag/AgCl
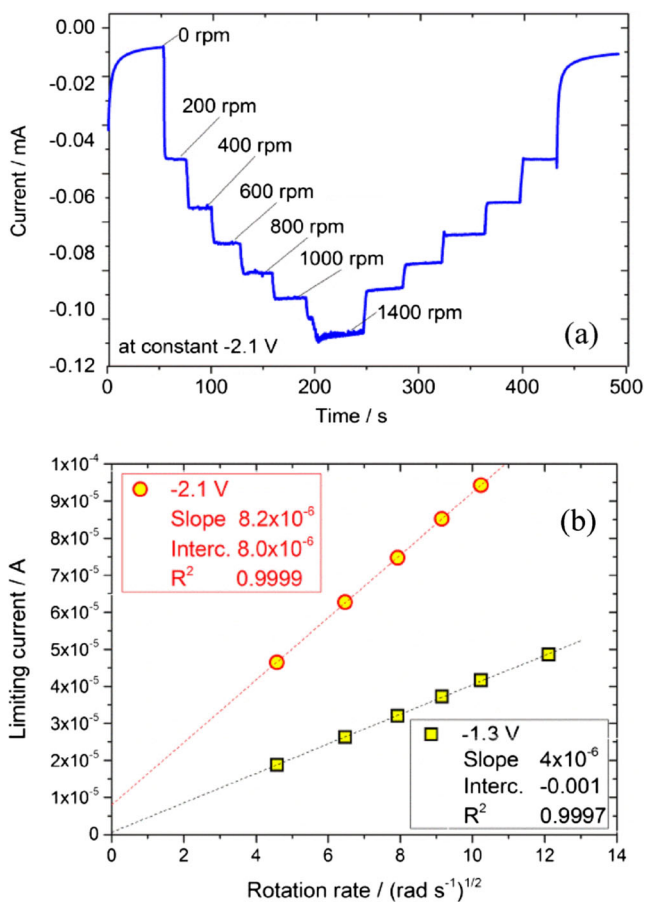
Fig. 9 a Staircase rotating disk electrode measurements with stepwise increase of the rotation rate from 0 to 1400 rpm, respectively, and a decrease to 0 rpm again at constant potential of −2.1 V vs. Ag/AgCl. Measurements are taken in DMF with 0.5 mM rhenium complex, 0.1 M TPABF$_4$, a glassy carbon working electrode, platinum wire counter electrode, and Ag/AgCl reference. b Levich plot for the measurements depicted in a and in the Fig. S1 at −1.3 and −2.1 V vs. Ag/AgCl

Fig. 10 Cyclic voltammograms of a homogeneous solution of (1) in nitrogen (*black line with squares*)- and CO$_2$ (*red line with circles*)-saturated electrolyte solution on a glassy carbon working electrode and b Pt as working electrode. The scan with CO$_2$ saturation shows a large current enhancement due to a catalytic reduction of CO$_2$ to CO. Measurements are taken at 50 mV s^{-1} in DMF with 0.1 M TPABF$_4$ (a) and 0.1 M TBAPF$_6$ (b), Pt counter electrode, and a catalyst concentration of 0.5 mM

catalytically enhanced under CO$_2$ atmosphere as can be seen in Fig. 10. Measurements are taken under otherwise identical conditions as described for previous measurements in Fig. 8. The current obtained for each rotation speed increases with increasing rotation speed as expected. The current reaches a stable plateau once the chosen rotation speed is reached. By lowering the rotation rate again from 1400 rpm after 250 s of measurement time, the current values follow exactly the initially obtained values when the rotation rate was increased, showing the reproducibility of these measurements.

The same experiment as shown in Fig. 9a but for a constant potential at −1.3 V, addressing the first plateau of the limiting current in the RDE experiments, can be seen in Fig. S1 in the supplementary information. In Fig. 9b, a Levich plot for the measurements depicted in (a) and in Fig. S1 at −1.3 and −2.1 V vs. Ag/AgCl is shown.

It is found that the slope of the Levich plot in Fig. 9 is about two times steeper for the current at the negative end (−2.1 V) addressing the fourth reduction peak compared to the second
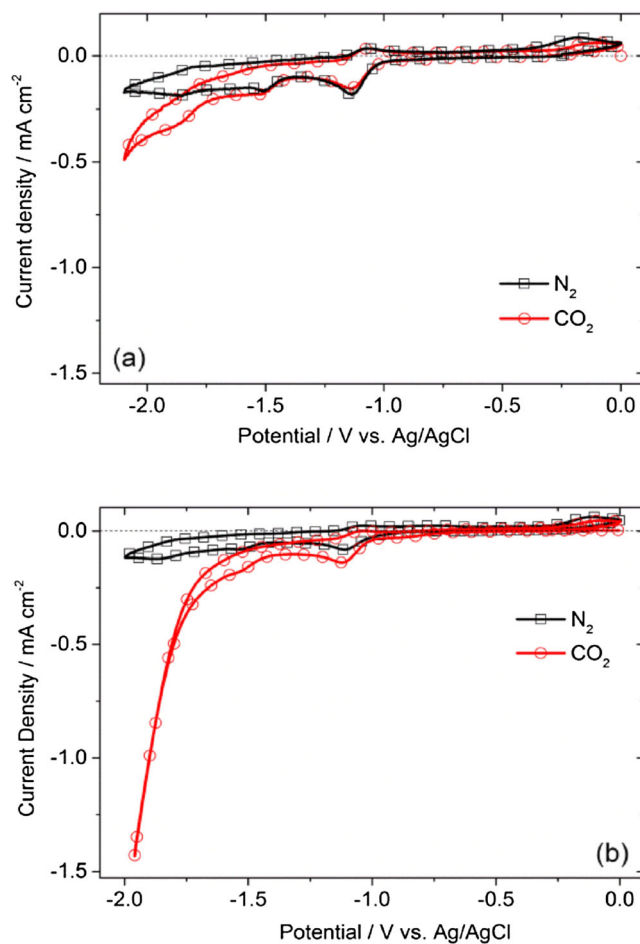
reduction peak (−1.3 V). Since it is the same diffusing species (1), the diffusion coefficient should not be significantly different, even with one additional electron. Therefore, the difference of the slope gives the number of electrons involved in the reduction process, resulting in two electrons transferred per molecule at −2.1 V. This outcome supports the interpretation of the cyclic voltammogram data described above in Fig. 6 and according to the presented reactions (i) to (v).

From these data, the diffusion coefficient for this new type of catalyst material can be determined with $2.5(\pm 0.5) \times 10^{-6}$ cm^2 s^{-1}. Similar results have been reported for other catalyst metal-bipyridine complexes in literature [9, 39].

CO$_2$ Reduction

The data obtained for the diffusion coefficient from the RDE experiments can then be used, once the catalytic current under

CO$_2$ saturation is known, to evaluate the catalytic second-order rate constant for CO formation of compound (**1**). Figure 10 shows the cyclic voltammograms of (**1**) measured in N$_2$- and CO$_2$-saturated DMF solution, respectively, for a glassy carbon (Fig. 10a) and a Pt (Fig. 10b) working electrode. Under N$_2$-saturated conditions, (**1**) showed a similar behavior as already presented in Fig. 6 for the electrochemical characterization measurements.

When the DMF solution was saturated with CO$_2$, the compound (**1**) demonstrated a strong enhancement in the current density after the third reduction wave. As can be seen in the comparison between Fig. 10a, b, the nature of the working electrode has a big influence on the measured current density under CO$_2$ saturation, increasing threefold when Pt is used instead of glassy carbon. One reason for this behavior might be the activation capability of Pt on protons. This is known to positively influence the catalytic activity of Re-based catalysts for CO$_2$ reduction [18, 40]. It has been shown that addition of weak Brönsted acids increases the catalytic current of these systems. This is assumed to be due to a stabilizing effect of the Re-CO$_2$ adduct which might facilitate the cleavage of the C-O bond and results in CO formation [41]. For the measurement depicted in Fig. 10a, compound (**1**) showed a 2.4-fold, while in Fig. 10b, a 11-fold increase in current density at the fourth irreversible reduction wave under CO$_2$ at −1.9 V vs. Ag/AgCl.

Scan rate-dependent cyclic voltammograms of a homogeneous solution of (**1**) in CO$_2$-saturated electrolyte at 10, 50, and 100 mV s^{-1} are presented in Fig. S2a and the plot of the linear dependence of the cathodic peak current density with the square root of the scan rate in Fig. S2b in the supplementary information. The linearity indicates again a diffusion-limited electrochemical reaction for the CO$_2$-saturated case, showing the importance of the RDE experiments for determining the diffusion coefficient for the catalyst material (**1**).

Comparing this result to previously reported data on the compounds (**3**) and (**2**), it was found that (**3**) showed a strong enhancement in the second reduction wave current density where else for (**2**) a clear separation of the reduction waves could not be obtained. Furthermore, it has been reported that compound (**3**) showed a 4.5-fold increase in current density at the second irreversible reduction wave under CO$_2$ at −1.75 V (vs. NHE), while the first quasi-reversible reduction wave did not show a significant increase. The compound (**2**) showed a 6.5-fold increase in current density at the second irreversible reduction wave under CO$_2$ at −1.75 V (vs. NHE) [13]. With the data obtained for the diffusion coefficient of 2.5($\pm$0.2)$\times$ 10^{-6} cm^2 s^{-1} and the catalytic current from the measurement presented in Fig. 10, the catalytic second-order rate constant for CO formation using Eq. 3 was evaluated. Second-order rate constants for CO formation of about 30($\pm$3) M^{-1} s^{-1} on glassy carbon and 450($\pm$40) M^{-1} s^{-1} on Pt working electrode were obtained using this method.

Additionally, the following Eq. 4 can be used to determine the peak current (i_p) of a compound with a reversible electron transfer and no following reaction [37].

$$i_p = 0.446 n^{3/2} FA[cat] \sqrt{\frac{DF\nu}{RT}} \tag{4}$$

where ν is the applied scan rate. The ratio of i_c to i_p measured in the cyclic voltammetry experiments shown in Fig. 10 can then be used to estimate k mathematically by dividing Eqs. 3 and 4 resulting in Eq. 5 [42, 43].

$$\frac{i_c}{i_p} = \frac{1}{0.446} \sqrt{\frac{RT}{nF}} \sqrt{\frac{k[Q]^y}{\nu}} \tag{5}$$

This method is used frequently because it allows a fast estimate of k without the need of knowing the diffusion coefficient (D) of the substance.

With a value of 2.4 for the ratio of i_c to i_p measured for the compound (**1**) on a glassy carbon working electrode, Eq. 5 yields in a second-order rate constant of about 54($\pm$3) M^{-1} s^{-1}. With the value of 11 for the ratio of i_c to i_p for the measurement with the Pt working electrode, Eq. 5 yields a second-order rate constant of about 560($\pm$50) M^{-1} s^{-1}. These values are slightly higher compared to the data obtained from the measurements of the diffusion coefficient depicted above and reported values in the literature for similar compounds [25]. When the same equations were used for (**3**) and (**2**), second-order rate constants of about 60 and 220 M^{-1} s^{-1} were obtained, respectively [13].

Bulk electrolysis experiments for CO$_2$ reduction were carried out using an H-cell geometry with separated anode and cathode compartment. Figure 11a shows the current-time curve for a typical constant potential electrolysis experiment of (**1**) (0.5 mM) in CO$_2$-saturated electrolyte solution with Pt as working electrode at constant −1.9 V vs. Ag/AgCl. The total electrolysis time was 5 h. Headspace gas samples were taken for product analysis regarding the formation of CO. The spikes in the curve at 1 h 4 min, 1 h 54 min, and 3 h 35 min indicate the time when headspace gas samples were taken for gas chromatography (GC) analysis. The spikes originate from manually induced vibrations at the contact cables by taking the sample. The corresponding headspace GC measurements for carbon monoxide are shown in Fig. 11b where CO is observed with a typical retention time after 10.7 min.

It can be seen in Fig. 11b that the amount of CO formed increased continuously over the electrolysis time as expected. The faradaic efficiencies increased from initially 9.5 % after 1 h and 4 min to 12.7 % at the end of the 5-h electrolysis experiment. This can then also be recalculated in a turn-over number (TON) when the TON is considered merely as the number of turnovers completed at the moment when the amount of CO was quantified. Using this analysis, the TON
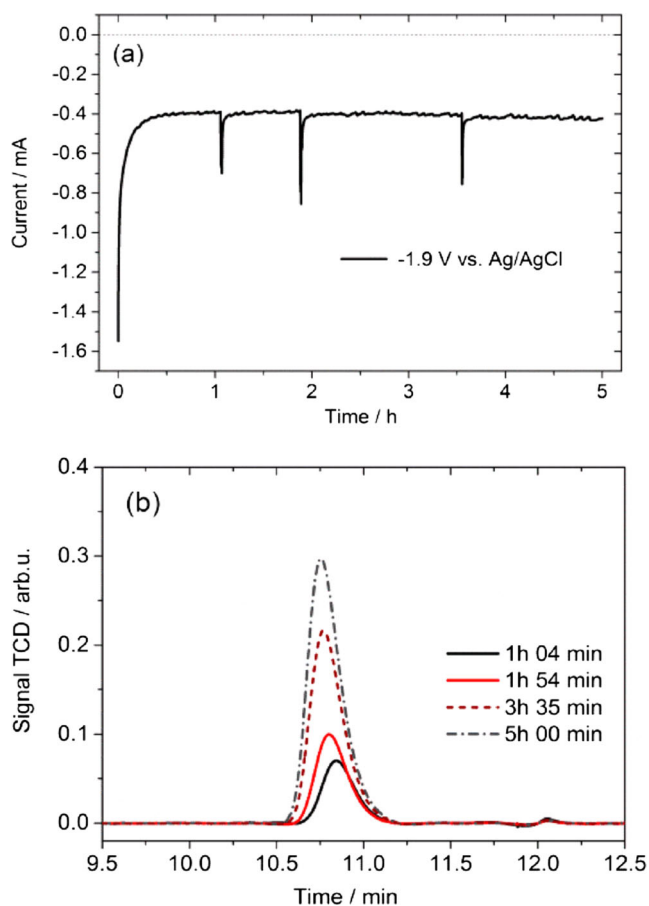
Fig. 11 In **a** the current-time curve for the constant potential electrolysis experiment of 0.5 mM (**1**) in CO_2-saturated electrolyte solution with Pt as working electrode at constant −1.9 V vs. Ag/AgCl for an electrolysis time of 5 h is shown. The *spikes* in the curve at 1 h 4 min, 1 h 54 min, and 3 h 35 min indicate the time when headspace gas samples were taken for GC analysis. **b** Corresponding headspace GC measurements after 1 h 4 min, 1 h 54 min, and 3 h 35 min and 5 h, for carbon monoxide with a typical retention time after 10.7 min

increases from initially 0.04 after 1 h and 4 min to 0.24 at the end of the 5-h electrolysis experiment. Although this is still below one, it has to be noted that, after an electrolysis time of 5 h now significant drop in the current-time curve was observed leading to the conclusion that the catalyst material still remained active. However, the color of the anode compartment turned dark orange which is attributed to oxidation products formed on the counter electrode, compare Fig. S3a in the supplementary information. Separate samples were taken from the anode and cathode compartment and analyzed with UV-vis absorption spectroscopy, compare Fig. S3b in the supplementary information.

The faradaic efficiencies for CO formation obtained at constant −1.9 V vs. Ag/AgCl are rather low. The measured values increase from 9.5 % after 1 h to around 12 % over an electrolysis time of 5 h. Previously reported values for similar compounds showed faradaic efficiencies close to 100 % [9, 25]. This leads to the conclusion that a substantial amount of

the depicted current is used by competing side reactions as for example the dimerization by forming a Re^0-Re^0 bond according to reaction (iii) or H_2 evolution [34]. However, the catalyst performance is surprisingly stable over an electrolysis time period of 5 h. It cannot be excluded that the experimental design has to be modified for an improved product analysis regarding the CO accumulation in this system. Future studies with improved electrolysis cells are currently under way to elucidate this issue. A detailed analysis of these measurements and the corresponding calculation of the faradaic efficiencies for CO formation can be found in Table S1 in the supplementary information.

Conclusion

In this study, the rhenium complex (**1**) has been fully characterized in terms of electrochemistry and spectroscopy. The measured results were compared to computational quantum mechanical calculations on the DFT level and to similar, previously reported rhenium complexes. It could be shown that the electrochemical and optical properties of this type of compounds are heavily influenced by modifications at the bipyridine ligand while the rhenium metal center remains active for electrochemical CO_2 reduction. The substitution in *para*-position to the metal binding site in addition to the situation in (**2**) leads to a more pronounced delocalization of π-electron density involving the central rhenium atom. This positively influences the catalyst activity towards electrocatalytic CO_2 reduction. Results showed an 11-fold increase in the current density under CO_2 saturation at a Pt working electrode and a catalytic second-order rate constant for CO formation of about 450(±40) M^{-1} s^{-1}, outperforming the benchmark compounds (**3**) and (**2**). Moreover, cyclic voltammetry measurements under CO_2-saturated electrolyte solution revealed a strong dependence on the nature of the working electrode. The positive effect of Pt is attributed to the availability of activated protons, which are known to positively influence the catalytic activity of Re-based catalysts. The presented results on (4,4′-bisphenylethynyl-2,2′bipyridyl)Re(CO)$_3$Cl in comparison with other organometallic rhenium(I) bipyridine complexes are important to further understand and improve the catalytic performance of these systems towards CO_2 reduction.

Experimental Section

General Experimental Procedures

Unless otherwise stated, all chemicals and solvents were purchased from commercial suppliers in reagent- or

technical-grade quality and used directly as received without further purification.

Synthesis

NMR spectra were recorded on Bruker digital Avance III NMR spectrometers (300 MHz). (4,4′-bisphenylethynyl-2,2′-bipyridyl)-Re(CO)$_3$Cl (1) ^{1}H NMR: (300 Hz, CDCl3): δ= 7.80–8.06 (10 H, m), 10.85–10.86 (2 H, d, J=4.62), 11.09 (1 H, s), 11.49 (1 H, s), 13.09–13.11 (2 H, d, J=86).

High-resolution mass spectra were recorded on an Agilent Q-TOF 6520 operated with ESI in both positive and negative mode.

(4,4′-bisphenylethynyl-2,2′-bipyridyl)-Re(CO)$_3$Cl (1): ESI-Pos. Calc. $(C_{29}H_{16}ClN_2O_3Re)Na^+$ [m/z (%)]: 683.0271 (48.8 %) 684.0304 (15.8 %) 685.0291 (100 %) 686.0323 (31.8 %) 687.0284 (31.7 %) 688.0308 (9.2 %) 689.0335 (1.6 %).

Found [m/z (%)]: 683.0269 (45.2 %) 684.0274 (14.5 %) 685.0285 (100 %) 686.0327 (29.0 %) 687.0267 (28.5 %) 688.0293 (8.2 %) 689.0357 (1.4 %).

ESI-Neg. Calc. $(C_{29}H_{16}ClN_2O_3Re)^{\bullet-}$ [m/z (%)]: 660.0384 (48.8 %) 661.0417 (15.8 %) 662.0404 (100 %) 663.0436 (31.8 %) 664.0397 (31.7 %) 665.0421 (9.2 %) 666.0448 (1.6 %) 667.0476 (0.2 %) 668.0503 (0 %).

Found [m/z (%)]: 660.0371 (48.5 %) 661.0408 (15.9 %) 662.0393 (100 %) 663.0423 (32.1 %) 664.0384 (32.3 %) 665.0406 (9.6 %) 666.0244 (8.3 %) 667.0334 (0.8 %) 668.0402 (0.3 %).

The high-resolution mass spectra can be found in Fig. S6 in the supplementary information.

Electrochemistry

Electrochemical experiments were performed using a JAISSLE Potentiostat-Galvanostat IMP 88 PC. A one-compartment cell was used for cyclic voltammetry experiments with a glassy carbon or Pt working electrode, a Pt counter electrode, and a Ag/AgCl quasi-reference electrode (QRE) calibrated with ferrocene/ferrocenium (Fc/Fc$^+$) as an internal reference. The half-wave potential ($E_{1/2}$) for Fc/Fc$^+$ was measured at 426 mV vs. QRE.

Rotating disk electrochemistry was performed on a Radiometer Analytical, EDI101 system in combination with a Hokuto Denko, HSV-110 potentiostat.

Controlled potential electrolysis experiments were performed in a gastight one-compartment and two-compartment cell with a Pt or glassy carbon working electrode, a Pt counter electrode, and a Ag/AgCl quasi-reference electrode using ferrocene (Fc/Fc$^+$) as an internal reference. The one-compartment cell contained 14 mL of electrolyte solution and 10 mL gas phase. The two-compartment cell contained 40 mL of electrolyte solution and 32 mL of gas phase in total.

The two compartments of the cell were separated by a glass drip.

It was found that the compound Re(4,4′-bisphenylethynyl-2,2′bipyridyl)(CO)$_3$Cl was purely soluble in most common organic solvents like acetonitrile (ACN) or dimethylformamide (DMF). To obtain a homogenous solution, the mixture was put in an ultrasonic bath for approximately 30 min to fully dissolve the material. The Ag/AgCl reference electrode was prepared according to the reported procedure [44].

The catalyst concentration in all cyclic voltammogram experiments was 0.5 mM, and the CO$_2$ concentration was assumed to be at gas saturation of 0.175 M in DMF [45].

Spectroscopic Methods

UV-vis spectroscopy scans were taken on a PerkinElmer LAMBDA 1050 double monochromator spectrometer (source doubling mirror) between 400 and 700 nm in 2-nm steps, with a slit width of 2 nm and a detector response time of 0.2 s. Signal to noise was optimized by attenuating the reference beam with internal attenuators (automatic 2A and 3A attenuation). For all spectra, autozero (100 and 0 %) correction scans were taken (baseline correction). The spectrometer is equipped with a deuterium (D2) lamp as the UV and a tungsten lamp as the visible and NIR source. The energy is dispersed into specific wavelengths by the use of a reflective grating. The source change is set to 320 nm. Photomultiplier R6872 and PMT for detection in the UV/vis, a Peltier cooled InGaAs detector for use in the 800–2600 nm region, and a Peltier cooled PbS detector for the range from 2500 to 3300 nm.

Photoluminescence (PL) spectra were recorded on a PTI QuantaMaster™ 400 spectrofluorometer with a continuous Xenon arc lamp (75 W) light source emission range from 185 to 680 nm, a Czerny-Turner type excitation monochromator (throughput 65 % at 300 nm) with a focal length of 300 mm, a excitation grating with 1200 line/mm (300 nm blaze), emission grating with 200 line/mm (400 nm blaze), and a multimode PTI PMT detector model 914, with a spectral response from 185 to 900 nm (Quantum Efficiency at 260 nm (Peak) 25.4 % typ.).

Infrared measurements were performed on a Bruker IFS 66/S FTIR spectrometer at room temperature in transmission mode, using a mercury-cadmium telluride (MCT) detector cooled with liquid nitrogen prior to the measurements.

GC Product Analysis

Gas chromatography (GC) analysis was conducted on a Thermo Trace GC equipped with a TCD detector and TG-WAXMS (30 m, 0.32 mm ID, 1 μm film) column. Carrier gas was helium at 20 mL min^{-1}, the GC was programmed from 30

(2) to 130 °C (8 min) with a heating rate of 10 °C min^{-1}. The injector was operated at 200 °C and the detector at 200 °C. Two-milliliter sample was injected with a gastight syringe directly from the headspace of the reaction vessel.

Conflict of Interest The authors declare no competing financial interests.

References

1. A. Kerr, Richard, Science (80) 317–437 (2007)
2. P. Friedlingstein, Nature **451**, 297–8 (2008)
3. K.M.K. Yu, I. Curcic, J. Gabriel, S.C.E. Tsang, ChemSusChem **1**, 893–9 (2008)
4. V. Balzani, A. Credi, M. Venturi, ChemSusChem **1**, 26–58 (2008)
5. B. Kumar, M. Llorente, J. Froehlich, T. Dang, A. Sathrum, C.P. Kubiak, Annu. Rev. Phys. Chem. **63**, 541–69 (2012)
6. N.S. Spinner, J.A. Vega, W.E. Mustain, Catal. Sci. Technol. **2**, 19 (2012)
7. H. Takeda, K. Koike, H. Inoue, O. Ishitani, J. Am. Chem. Soc. **130**, 2023–31 (2008)
8. K. Koike, S. Naito, S. Sato, Y. Tamaki, O. Ishitani, J. Photochem, Photobiol. A Chem. **207**, 109–114 (2009)
9. J.M. Smieja, C.P. Kubiak, Inorg. Chem. **49**, 9283–9 (2010)
10. E. Portenkirchner, K. Oppelt, D.A.M. Egbe, G. Knör, N.S. Sariciftci, Nanomater Energy **2**, 134–147 (2013)
11. K. Oppelt, D.A.M. Egbe, U. Monkowius, M. List, M. Zabel, N.S. Sariciftci, G. Knör, J. Organomet. Chem. **696**, 2252–2258 (2011)
12. H. Takeda, K. Koike, T. Morimoto, Inorg. Photochem. **63**, 137–186 (2011)
13. E. Portenkirchner, K. Oppelt, C. Ulbricht, D.A.M. Egbe, H. Neugebauer, G. Knör, N.S. Sariciftci, J. Organomet. Chem. **716**, 19–25 (2012)
14. D.A.M. Egbe, B. Heise, E. Klemm, Des. Monomers Polym. **3**, 289–297 (2000)
15. G.-J. ten Brink, I.W.C.E. Arends, M. Hoogenraad, G. Verspui, R.A. Sheldon, Adv. Synth. Catal. **345**, 497–505 (2003)
16. H. Staats, F. Eggers, O. Haß, F. Fahrenkrug, J. Matthey, U. Lüning, A. Lützen, Eur. J. Org. Chem. **2009**, 4777–4792 (2009)
17. J. Hawecker, J. Lehn, R. Ziessel, J. Chem. Soc. Chem. Commun. **6**, 328–330 (1984)
18. J. Hawecker, J. Lehn, R. Ziessel, Helv. Chim. Acta **69**, 1990–2012 (1986)
19. K.A. Walters, Y.-J. Kim, J.T. Hupp, Inorg. Chem. **41**, 2909–2919 (2002)
20. K.D. Ley, K.S. Schanze, Coord. Chem. Rev. **171**, 287–307 (1998)
21. Y. Liu, Y. Li, K.S. Schanze, Photochem. Photobiol. **3**, 1–23 (2002)
22. M.D. Sampson, J.D. Froehlich, J.M. Smieja, E.E. Benson, I.D. Sharp, C.P. Kubiak, Energy Environ. Sci. **6**, 3748 (2013)
23. K. A. Grice, C. P. Kubiak, Recent studies of rhenium and manganese bipyridine carbonyl catalysts for the electrochemical reduction of CO$_2$, Elsevier Inc. (2014)
24. E. Portenkirchner, J. Gasiorowski, K. Oppelt, S. Schlager, C. Schwarzinger, H. Neugebauer, G. Knör, N.S. Sariciftci, ChemCatChem **5**, 1790–1796 (2013)
25. L.G. Wade, *Organic Chemistry* (Prentice-Hall, Englewood Cliffs, 1987)
26. A.P. Scott, L. Radom, J. Phys. Chem. **100**, 16502–16513 (1996)
27. L. Yang, A.-M. Ren, J.-K. Feng, X.-D. Liu, Y.-G. Ma, H.-X. Zhang, Inorg. Chem. **43**, 5961–72 (2004)
28. D. J. F. M. J. Frisch, G. W. Trucks, H. B. Schlegel, G. E. Scuseria, M. A. Robb, J. R. Cheeseman, G. Scalmani, V. Barone, B. Mennucci, G. A. Petersson, H. Nakatsuji, M. Caricato, X. Li, H. P. Hratchian, A. F. Izmaylov, J. Bloino, G. Zheng, J. L. Sonnenberg, M. Had, (2009)
29. A.D. Becke, Phys. Rev. A **38**, 3098–3100 (1988)
30. C. Lee, W. Yang, R.G. Parr, Phys. Rev. B **37**, 785–789 (1988)
31. W.J. Hehre, J. Chem. Phys. **56**, 5255 (1972)
32. V.A. Rassolov, M.A. Ratner, J.A. Pople, P.C. Redfern, L.A. Curtiss, J. Comput. Chem. **22**, 976–984 (2001)
33. P.J. Hay, W.R. Wadt, J. Chem. Phys. **82**, 270 (1985)
34. A.I. Breikss, H.D. Abruña, J. Electroanal, Chem. Interfacial Electrochem. **201**, 347–358 (1986)
35. C.H. Hamann, A. Hamnett, W. Vielstich, *Electrochemistry* (WILEY-VCH, Weinheim, 1998)
36. V.G. Levich, Acta Physicochim. URSS **17**, 257–307 (1942)
37. A. J. Bard, L. R. Faulkner, Electrochemical methods: fundamentals and applications, WILEY-VCH, (2000)
38. J.M. Saveant, E. Vianello, Electrochim. Acta **8**, 905–923 (1963)
39. R.J. Haines, R.E. Wittrig, C.P. Kubiak, Inorg. Chem. **33**, 4723–4728 (1994)
40. J.M. Smieja, M.D. Sampson, K.A. Grice, E.E. Benson, J.D. Froehlich, C.P. Kubiak, Inorg. Chem. **52**, 2484–91 (2013)
41. K. Wong, W. Chung, C. Lau, J. Electroanal. Chem. **453**, 161–169 (1998)
42. D.L. Dubois, A. Miedanerlt, R.C. Haltiwangert, J. Am. Chem. Soc. **113**, 8753–8764 (1991)
43. A. Miedaner, C.J. Curtis, R.M. Barkley, D.L. Dubois, Inorg. Chem. **33**, 5482–5490 (1994)
44. A.W. Hassel, K. Fushimi, M. Seo, Electrochem. Commun. **1**, 180–183 (1999)
45. B. P. Sullivan, Electrochemical and electrocatalytic reactions of carbon dioxide, Elsevier, (1993)